Impact of the sequence of precursor introduction on the growth and properties of atomic layer deposited Al-doped ZnO films

Harold Le Tulzo, Nathanaelle Schneider, Daniel Lincot, Gilles Patriarche, Frédérique Donsanti

Impact of the sequence of precursor introduction on the growth and properties of atomic layer deposited Al-doped ZnO films

Harold Le Tulzo, Nathanaelle Schneider, Daniel Lincot, Gilles Patriarche, and Frédérique Donsanti

Citation: Journal of Vacuum Science & Technology A **36**, 041502 (2018); doi: 10.1116/1.5030990
View online: https://doi.org/10.1116/1.5030990
View Table of Contents: http://avs.scitation.org/toc/jva/36/4
Published by the American Vacuum Society

Impact of the sequence of precursor introduction on the growth and properties of atomic layer deposited Al-doped ZnO films

Harold Le Tulzo[a)]
Institut Photovoltaïque Ile de France (IPVF), 30 route départementale 128, 91120 Palaiseau, France and French Environment and Energy Management Agency (ADEME), 20 avenue du Grésillé, 49004 Angers, France

Nathanaelle Schneider and Daniel Lincot
Institut Photovoltaïque Ile de France (IPVF), 30 route départementale 128, 91120 Palaiseau, France and CNRS, Institut Photovoltaïque Ile de France (IPVF), UMR 9006, 30 route départementale 128, 91120 Palaiseau, France

Gilles Patriarche
Centre de Nanosciences et de Nanotechnologies, CNRS, Université Paris Sud, Université Paris Saclay, route de Nozay, 91460 Marcoussis, France

Frédérique Donsanti
Institut Photovoltaïque Ile de France (IPVF), 30 route départementale 128, 91120 Palaiseau, France and EDF R&D, 30 route départementale 128, 91120 Palaiseau, France

(Received 27 March 2018; accepted 22 May 2018; published 18 June 2018)

Atomic layer deposition relies on surface chemical reactions which implies that the order of the precursor pulses (so-called "sequence") impacts the growth, especially for multinary compounds. In the case of Al-doped zinc oxide (AZO) thin films, the sequence of introduction of precursors trimethyl aluminum (TMA)/diethylzinc (DEZ)/H_2O has been reported to impact their growth and some of their properties. Here, five different Al sequences for doping the AZO films in Al have been tested at a constant deposition temperature of 160 °C and a TMA:DEZ ratio of 1:10, and the film growth and properties are investigated by *in situ* quartz crystal microbalance (QCM) measurements and *ex situ* characterizations. This paper provides evidence of the impact of the Al sequence on AZO material and proposes an explanation of the macroscopic properties based on the nature of chemical surface reactions evidenced by QCM. The growth rate, composition, electrical and optical properties, and, to a lesser extent, structural properties are affected by the TMA/DEZ/H_2O pulse sequence. In particular, better electrical properties are obtained by reducing the Al content incorporated per cycle when the TMA pulse follows a DEZ pulse and, second, the optical band gap size is increased when the TMA pulse is between two DEZ pulses. Mass variations during surface reactions of TMA on hydroxyl and zinc-alkyl surface groups have also been proven to be temperature dependent when comparing growth mechanisms at 160 and 200 °C. It is also observed that the increase in temperature has a similar impact on the mass variations as the increase in the TMA:DEZ ratio. This is probably because of an improved intermixing between Al species and ZnO layers. *Published by the AVS.* https://doi.org/10.1116/1.5030990

I. INTRODUCTION

The wide direct band gap low-cost semiconductor ZnO, composed of nontoxic and abundant raw materials, is a promising transparent conductive oxide[1–4] that particularly retains attention in the solar cell field.

A main advantage of ZnO is the possibility to tune its optoelectronic properties by doping (band gap size can be widened and resistivity lowered). Various dopant atoms have already been tested, including Al, B, F, Ga, H, In and S (Refs. 3–5) that must be controlled in concentration and distribution. Among them, aluminum is one of the most used n-type dopant which generates a n-type semiconductor, usually called Al-doped ZnO (AZO). However, some challenges remain such as preventing damages on the bottom layers upon deposition[6] or the slow diffusion of aluminum in oxide at a low temperature[7] that deteriorates the electrical properties. Thus, the deposition method must be chosen carefully to obtain the desired film quality under conditions compatible with the substrate. Until now, many fabrication methods have been employed to prepare AZO including sol-gel processes,[8] spray pyrolysis,[9] magnetron sputtering,[4] pulse laser deposition,[4] metal organic chemical vapor deposition,[4] atomic layer deposition (ALD),[10] and molecular beam epitaxy.[11] Among them, magnetron sputtering is mostly used as it is fast (0.01–2 nm/s) and leads to low resistive AZO films (2×10^{-4} Ω cm for 425–650 nm films). Nevertheless, it can damage the bottom layers and the film conformality on high aspect ratio structures is poor. To avoid this, ALD method is promising, not only because conformal, pinhole free and dense materials can be obtained, but also because low resistivities are reported ($5–6 \times 10^{-4}$ Ω cm).[12–16] In ALD, in comparison to CVD, gases called precursors are injected successively, rather than simultaneously, inside a reactor and

a)Electronic mail: harold.le-tulzo@chimieparistech.psl.eu

react with the substrate or upon the already deposited film. As the reaction stops when the surface is saturated, these self-limiting surface chemical reactions allow a controlled growth at the angstrom scale. By exploiting the unique properties of ALD, specific ultrathin film deposition on 3D structures is possible.[17] Moreover, as a relative low temperature deposition method ($T < 250\,^{\circ}C$), it is suitable for organic based devices fabrication.[18] ALD is also particularly well-adapted to synthesize doped materials as it allows a precise control of the doping level.

ALD is increasingly investigated to deposit ZnO thin films or nanostructures. Typically, diethylzinc [DEZ, $Zn(C_2H_5)_2$] and deionized water (H_2O) are used as precursors of Zn and O atom sources. In the case of AZO deposition, Zn-O cycles are often combined with Al-O cycles and tri-methyl aluminum [TMA, $Al(CH_3)_3$] is commonly used as the Al source. The usual order of precursor introduction alternates an organometallic pulse (DEZ or TMA) with a water pulse, such as DEZ/H_2O/TMA/H_2O/DEZ/H_2O. The reported optimal Al atomic doping ratio varies in the [2; 5] % range.[10] This optimal range value is not always determined by elemental analytical techniques, but rather corresponds to the expected doping level of Al calculated from the ratio of the growth per cycle or the number of cycles of Al_2O_3 and ZnO which may differ from the experimental Al doping level. Controlling the Al doping level can be achieved by varying the Al-O/Zn-O ratio,[10] the deposition temperature,[10,19] and the pulse[20] or purge[21,22] duration times, by coinjecting the Zn and Al precursors,[23] or by using an alternative Al precursor such as $Al(CH_3)_2(O^iPr)$[24] or $Al(OiPr)_3$.[25,26] Another solution is to use different orders of precursor introduction for doping the film in Al (referred to as "Al sequence"), such as DEZ/TMA/H_2O sequence for which DEZ and TMA pulses are only separated by a N_2 purge step[13,27–29] versus the usual TMA/H_2O sequence. This latter solution can improve the distribution of Al atoms, reduce the formation of nanolaminate structures, and lead to better optoelectronic properties of AZO films. However, thus far, only a few articles compare the influence of the Al sequence on the film growth and properties. For example, Na *et al*. reported *in situ* quartz crystal microbalance (QCM) results for three Al sequences with three different [pulse number of TMA]:[pulse number of DEZ] ratios (T:D ratio).[30] They highlighted that the chemical interactions between Zn and Al species depend on the Al sequence as well as on the T:D ratio. In addition, film growth and overall final properties were also proved to be impacted by the Al sequence. Pollock and Lad mainly focused on the structure and resistivity of the resulting AZO films grown with three Al sequences for 1:11 or 1:12 T:D ratios.[31] One of these three Al sequences was evidenced as leading to the lowest resistive film independent of the thickness, the crystallographic texture, and the grain size. In this paper, we explored the influence of the Al sequence on the film properties for a deposition temperature of 160 °C. For this, five Al sequences (detailed in Fig. 1) were tested at a fixed T:D ratio (1:10) and their effects on the growth and properties of AZO films were discussed by means of *in situ* QCM measurements and *ex situ* films characterizations. The selected 1:10 ratio in this comparative work is more appropriate than lower ones as it enables an increase in the difference of properties between films based on an enhanced impact of the doping. Correlations between these properties are highlighted to understand the growth mechanisms.

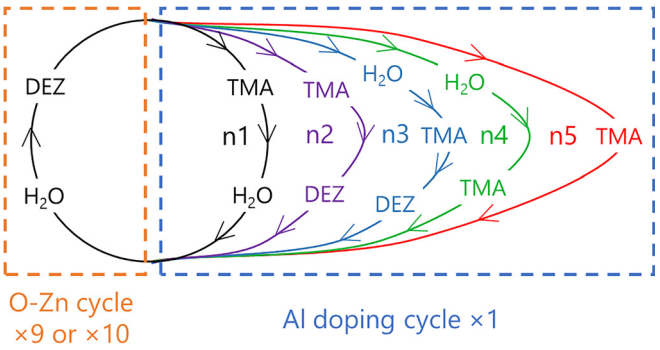

FIG. 1. (Color online) Schematic representation of the five Al sequences investigated. Films were grown with a TMA:DEZ ratio of 1:10.

II. EXPERIMENT

A. Thin film synthesis and *in situ* growth characterization

1. Atomic layer deposition of AZO thin films

AZO thin films were prepared at deposition temperature $T_{dep} = 160\,^{\circ}C$ using a BENEQ TFS-200 ALD reactor. High purity nitrogen 99.9999% (Air Liquide) was used as carrier and purge gas. The carrier gas flow rate was set at 600 sccm. In the reaction chamber, the pressure was kept around 1 mbar. DEZ (EpiPure, SAFC), TMA (Optograde, Rohm & Haas), and deionized water were used as Zn, Al, and O precursors, respectively, at room temperature. Thin films were deposited simultaneously on borosilicate glass (SCHOTT Borofloat 33) and on n-doped Si (100) wafer with native oxide top layer. Prior to deposition, borosilicate glass substrates were washed at room temperature by sonification in acetone and iso-propanol (2×5 min), and Si (100) substrates washed in a detergent solution (RBS 35 concentrate, 2% in water, 5 min) at room temperature and rinsed with deionized water. A O-Zn growth cycle was achieved via the following procedure: H_2O pulse/N_2 purge/DEZ pulse/N_2 purge with pulse times of 0.1 s and purge times, respectively, equal to 1 and 0.7 s. Five different Al sequences, defined as the order of the precursor pulses during the Al doping cycle, were grown and correspond to TMA/H_2O (n1 sequence), TMA/DEZ (n2 sequence), H_2O/TMA/DEZ (n3 sequence), H_2O/TMA (n4 sequence), and TMA (n5 sequence) (see Fig. 1). During these Al doping cycles, DEZ pulse/purge times and H_2O pulse time were kept at 0.1/0.7 and 0.1 s, TMA pulse/purge times set at 0.15/0.5 s. H_2O purge time was either 1 s (when pulsed before TMA) or 0.75 s (when pulsed after TMA). In one supercycle, the Al doping cycle was interspersed with 9 or 10 O-Zn growth cycles to keep constant the [pulse number of TMA]:[pulse number of DEZ] ratios (referred as "T:D ratio") to 1:10. The number of cycles (n)

was set to have a constant number of metal pulse leading to n = 440 for sequences n1, n4, n5, and n = 400 for sequences n2, n3. To refer to the film grown by one of the Al sequence, "nx-film" is employed with x the sequence number, such as n1-film is the AZO film grown with the sequence n1.

2. In situ *QCM measurements*

In situ QCM measurements were acquired with a Colnatec Eon-LT monitor system, using a HT quartz crystal covered by an alloy (6 MHz initial oscillation frequency) located on the cover lid of the reactor. The signal was recorded every 0.2 s, and the lowest thickness step precision was 0.04 Å. Measurements were done after a stabilization time in order to reach a uniform and constant temperature in the whole reaction chamber ($\Delta T \pm 1.5\,^{\circ}C$). QCM experiments were conducted at $T_{dep} = 160\,^{\circ}C$ for the five Al sequences and at $T_{dep} = 200\,^{\circ}C$ only for n1 and n3 sequences. To account for the larger reactor volume in QCM configuration and to ensure an effective saturation state, longer pulse (0.5 s) and purge times (5 s) were chosen. Each deposition was performed on a 10 nm Al_2O_3 thick film used as the substrate layer for the growth of each AZO films. An average over five AZO supercycles were done in order to improve the measurement precision. *In situ* measurements for the five Al sequences have been normalized in order to obtain a similar ratio [GPC(AZO)]:[GPC(ZnO)] than with *ex situ* analysis. Mass were calculated from the thickness value by considering a density of 5.61 g/cm^3 (typical density of ALD-ZnO films).[32]

B. Thin film characterization

Film thicknesses were determined from samples deposited on glass substrates by x-ray reflectivity using a PANalytical Empyrean equipment. Fitting of the experimental curves were performed with X'PERT REFLECTIVITY software. Homogeneity of the samples has been verified on a 10×10 cm glass substrate. Thickness differences less than 2% relative were measured. The structural properties were monitored on the same equipment in the grazing incidence x-ray diffraction (GIXRD) condition with Cu Kα radiation. The electrical properties of the films deposited on glass were determined with a Hall effect measurement system (Ecopia HMS-3000), by van-der-Pauw method at room temperature in a magnetic field of 0.55 T. The values given for carrier concentration, mobility, and resistivity is an average of five measurements. The resistivity values were confirmed by a four-point probe measurement (Microworld Pro4). Optical transmittance and reflectance were obtained with a PerkinElmer Lambda 900 ultraviolet-visible-near infrared (UV-Vis-NIR) spectrophotometer system. The Al and Zn contents of the AZO thin films deposited on Si (100) wafer were investigated with energy dispersive X-ray spectroscopy (EDS) (Bruker Xflash 6130) installed on a field-emission scanning electron microscopy (ZEISS Merlin VP Compact). The electron beam acceleration voltage was set at 15 kV. The relative %Al/(%Al + %Zn) ratio is compared among the AZO films with the five different Al sequences. TEM/STEM studies were performed on a FEI Titan Themis 200 working at 200 kV with a geometrical aberration corrector on the probe (STEM mode). The probe resolution is about 0.1 nm and the probe current 85 pA. The microscope is equipped with a Ceta 16M camera for the TEM images and also with a SuperX system with four detectors for EDS analysis and the detected solid angle is 0.8 steradian (detection limit about 0.1 at. % for heavy elements such as Si or Zn). The TEM thin foils have been prepared by Ga focused ion beam (FIB) milling and their zone axes were aligned following a ⟨110⟩ direction of the silicon substrate. The surface of the samples have been protected by an amorphous carbon coating before the local platinum deposition in the FIB.

III. RESULTS

To explore the influence of the Al sequence on the film growth mechanism and properties, AZO thin films obtained from five different Al sequences (as depicted in Fig. 1), at a constant T:D ratio (1:10) and metal pulse numbers in their supercycles, were synthetized. Each growth process was followed *in situ* by QCM measurements, and the films were characterized.

A. Growth of AZO films

1. *Study of growth with* ex situ *thickness characterization*

To study the influence of the Al sequence on the film thicknesses, two distinct variables can be considered and are presented in Fig. 2. One is the growth per cycle (GPC, in Å/cycle), obtained by dividing the measured thickness by the number of ALD cycles. However, the number of TMA pulse (Al source) differs from one sequence to another: 400 for n2, n3 versus 440 for n1, n4, and n5. Moreover, according to previous studies, metal pulses (TMA or DEZ pulse) enable the more significant mass gain during ZnO and AZO growth.[30,33] Thus, we introduced another parameter, the growth per metallic pulse (GPMP, in Å/metallic pulse), which is the film thickness divided by the total number of metal pulses.

The Al sequence has an influence on both GPC and GPMP values. Those values are typically in the range of 1.45–1.7 Å/cycle for GPC, and 1.3–1.7 Å/cycle for GPMP and are all smaller than the ones of pure ZnO films (1.8 Å/cycle). Finally, GPMP and GPC values can be ranked for the five Al sequences as follows:

(1) GPMP: n4 > n1 ≈ n5 > n3 > n2,
(2) GPC: n4 > n3 > n1 ≈ n5 > n2.

2. *Study of growth with* in situ *measurements*

The mass variations relying on molecules adsorption and desorption during the AZO film depositions have been evidenced by recording *in situ* QCM measurements. Figure 3(a) displays the mass uptake variations over a whole supercycle for the five Al sequences. Average mass uptakes of [950; 1250] ng/cm^2 per supercycle are recorded depending on the

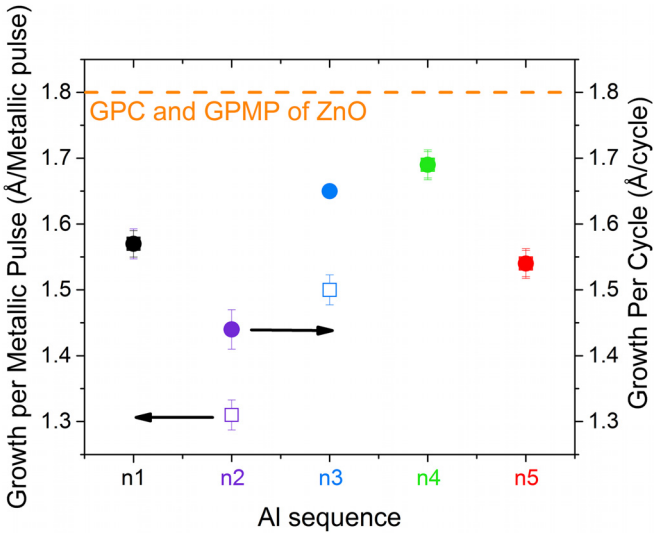

FIG. 2. (Color online) Influence of the Al sequence on the growth per cycle (GPC in Å/cycle, full circles) and GPMP (in Å/cycle, empty squares) of AZO films. The values obtained for ZnO films are plotted in dashed line. GPMP and GPC symbols are superposed for n1, n4, and n5 sequences.

Al sequence that correspond to an equivalent thickness comprised in [1.9; 2.2] nm. These thickness variation values obtained for one entire supercycle are higher than those obtained by *ex situ* characterization over the whole film as they do not take into account the nucleation phase on the quartz crystal covered by Al_2O_3 during which the growth rate is often smaller than during the steady growth phase.

Figure 3(b) illustrates the mass gained during each cycle of one AZO supercycle. The five curves are approximately superposed except for n2 curve which is lower than others that denotes a smaller mass uptake after each cycle of the supercycle. The upper and lower dotted lines correspond to the average mass uptake of undoped ZnO (120 ng/cm^2 per cycle or 2.13 Å/cycle) and Al_2O_3 (40 ng/cm^2 per cycle or 1.00 Å/cycle) films observed when grown at 160 °C whose values are consistent with the literature.[30,33] The mass uptake is not constant over the entire supercycle since the first O-Zn cycles show a reduced mass gain compared to the average mass uptake of undoped ZnO: 120 ng/cm^2 per cycle. The nucleation periods following the Al doping cycle is accounted for approximately 4–5 cycles meaning that 4–5 O-

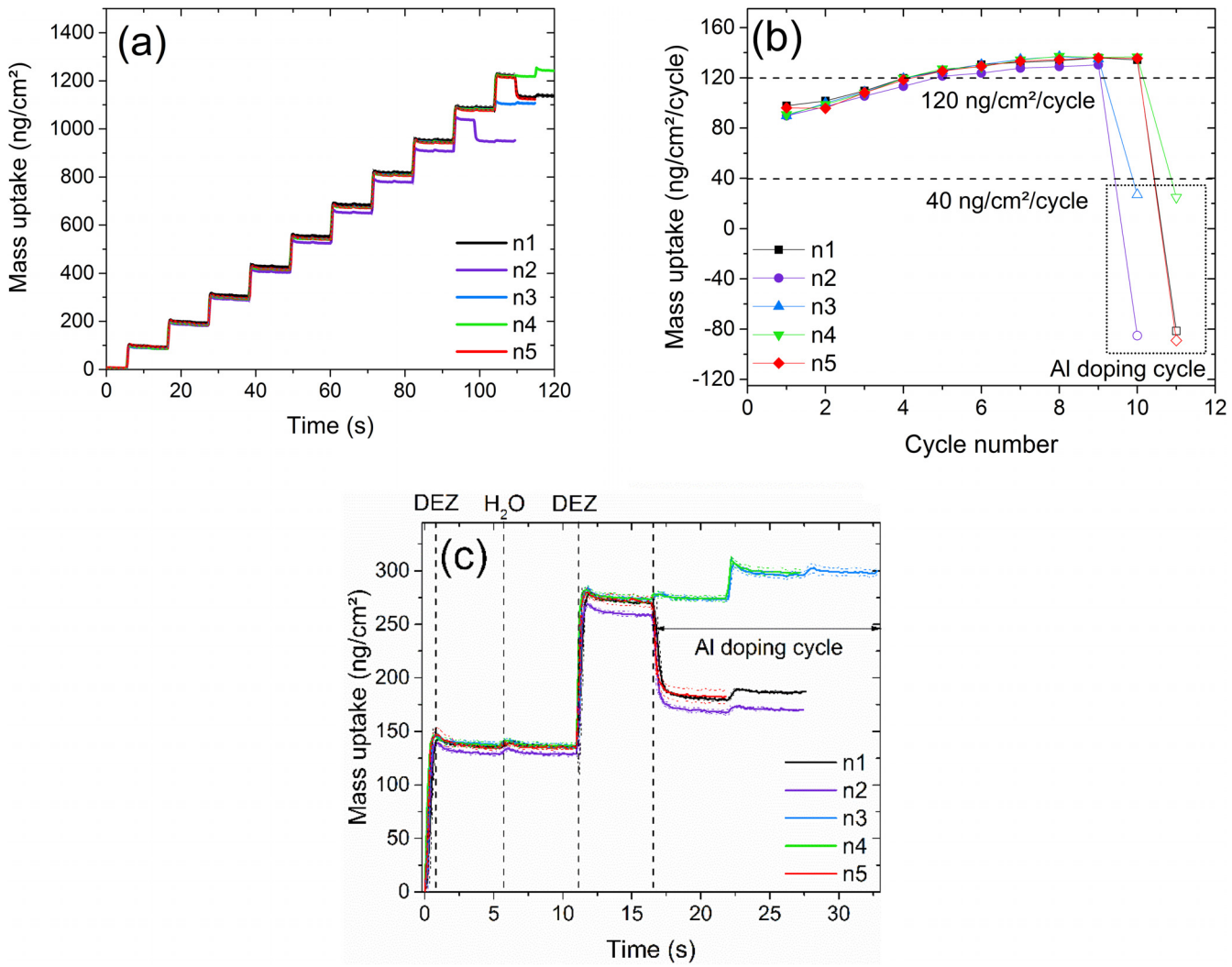

FIG. 3. (Color online) Mass uptake (a) as a function of the time over the entire supercycle; (b) as a function of the ALD cycle number; and (c) with a zoom on the Al doping cycle for AZO films grown with five sequences with a T:D ratio of 1:10 using *in situ* QCM measurements.

Zn cycles are necessary to recover a mass gain larger than 120 ng/cm^2 per cycle before a stagnation for the following cycles.[30,33] For all the Al sequences, the mass uptake is highly reduced during the Al doping cycle. For n3 and n4 sequences, it is closed to the average mass uptake of Al_2O_3 40 ng/cm^2 per cycle while for n1, n2, and n5, the net mass gain is negative, closed to −90 ng/cm^2 per cycle.

Variations during the five Al doping cycles have been emphasized and are shown on Fig. 3(c). During the O-Zn cycles, the mass is dominantly modified by DEZ pulses while H_2O pulses has only a small influence on the net mass change. All the Al sequences show similar mass uptake values until the beginning of the Al doping cycle except n2 sequence for which the mass uptake is lower. During the Al doping cycle, mass uptake relies on the pulse order and thus differs from one sequence to another. When the TMA pulse follows a DEZ pulse (n1, n2, and n5 sequences), a mass decrease in -90 ± 1 ng/cm^2 is observed that is lower than the mass increase obtained during the previous DEZ pulse ($+133 \pm 3$ ng/cm^2). When the TMA pulse follows a H_2O pulse (n3 and n4 sequences), a mass increase is recorded that corresponds to a [22; 24] ng/cm^2 gain that is inferior to the approximately +40 ng/cm^2 noted by Na *et al.*[30] A slight increase in mass is shown during the H_2O pulse following the TMA pulse for n1 sequence: +7.5 ng/cm^2 per cycle, and during the DEZ following the TMA pulse (n2 and n3 sequences): +2.8 ng/cm^2 per cycle for n2 and +2.5 ng/cm^2 per cycle for n3.

B. AZO film properties

1. Structural properties of AZO films

The structural properties of the films have been analyzed using GIXRD and their diffraction patterns and the main peak positions of AZO and ZnO films are presented in Fig. 4(a). All AZO films have similar diffraction patterns, which correspond to ZnO wurtzite phase. They appear as polycrystalline with (100), (101), and (110) crystallographic orientations. In comparison to the ZnO film of similar thickness, the diffraction peak at (002) is barely visible on AZO patterns, as reported at similar deposition temperatures[21,34] while its presence has already been evidenced for ALD processes at higher temperatures.[19,31]

Substitutional Al atoms are expected to induce a change in the lattice parameter. With GIXRD measurements, average distance between planes, d-spacing values, cannot be compared as all plane orientations are detected and not only the planes parallel to the surface.[35,36] Thus, to compare the Al incorporation, a discussion on peak positions was chosen and is presented in Fig. 4(b). The peaks on the AZO patterns that correspond to (100) and (110) diffraction planes show a shift compared to the peak positions on the ZnO pattern while the (101) peaks are closed to the same position. For the (100) and (110) main peaks, the ranking of peak position is the following from lowest to highest angular position:

$$(100) \rightarrow \text{n1} < \text{n5} = \text{n2} < \text{n4} < \text{n3},$$

$$(110) \rightarrow \text{n1} < \text{n2} < \text{n5} < \text{n4} < \text{n3}.$$

2. Compositional properties of AZO films

The atomic contents of all AZO films were determined by SEM-EDS measurements and the relative value of %Al/(%Al + %Zn), referred as aluminum fraction (AF_{SEM}) is presented on Fig. 5(a). All AF_{SEM} values except for n4 sequence differ from the value that can be expected from the T:D ratio [T:D = 1:10; %Al/(%Al + %Zn) = 9.1%]. Clear dependency of Al fraction on the sequence is observed, and AF_{SEM} can be ranked as followed: $AF_{n3} \approx AF_{n2} > AF_{n4} > AF_{n5} > AF_{n1}$.

EDS coupled with a TEM has been employed to determine the exact Al and Zn contents for two AZO films (n1 and n3), to assess the effective amount of Al and quantify the O content (Table I). Al, Zn, and O atoms are homogeneously distributed in the bulk of the films [see Fig. 5(b)], but a rich Al content is detected at the interface with Si. n3-film is oxygen rich and do not correspond to a Zn(Al)O stoichiometry [%O/(%Zn + %Al) = 1.17] while n1-film approximately respects the stoichiometry. In general, AF_{TEM}

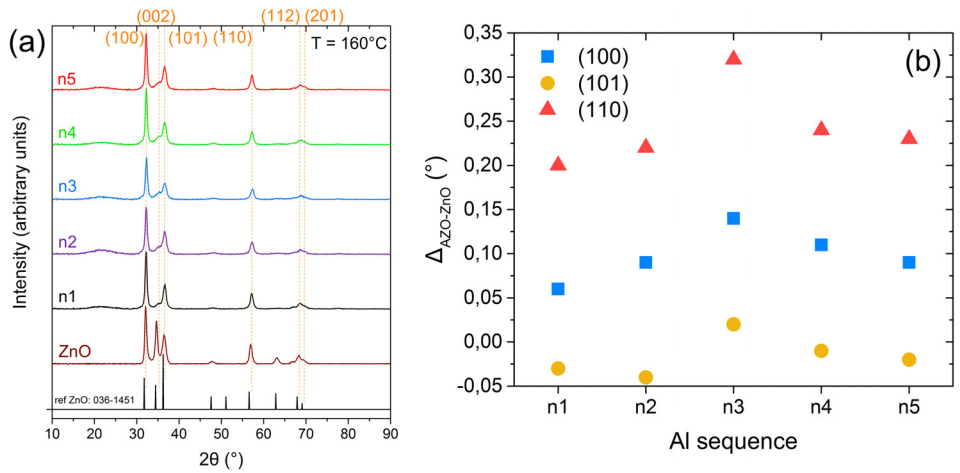

FIG. 4. (Color online) (a) GIXRD patterns of AZO (Al sequences n1–n5) and ZnO films ($T_{dep} = 160$ °C), along with the ZnO diffraction pattern (ICDD 00-036-1451). (b) Peak position difference between AZO and ZnO (in degrees) for the three main diffraction planes.

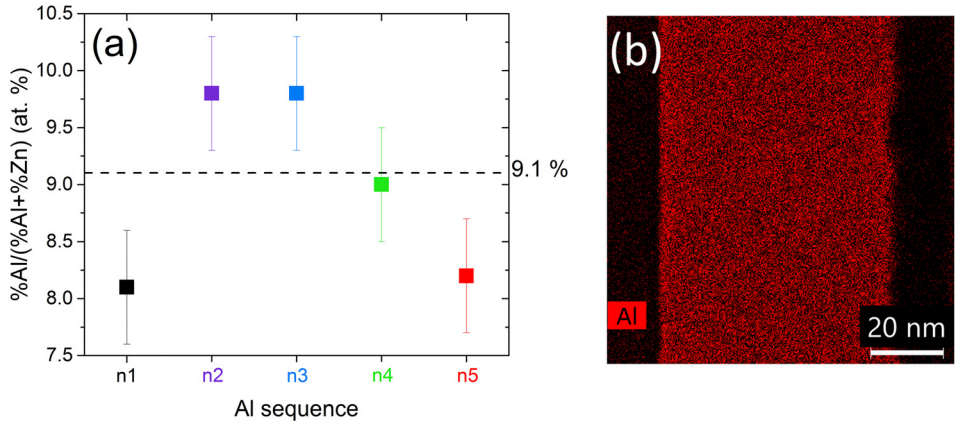

FIG. 5. (Color online) (a) Al fraction determined with SEM-EDS (AF_{SEM}) = %Al/(%Al + %Zn) for all AZO films (thickness = [57; 75] nm). Al fraction expected from the ratio T:D (AF = 9.1%) is represented by a dashed line on the graph. (b) Al distribution on EDS map of n3-film acquired by scanning TEM (EDS map on n1-film is similar).

values are significantly higher than AF_{SEM} ones, which means that they were underestimated from SEM-EDS. Still, in accordance with EDS-SEM measurements, the Al concentration exhibits a higher value for n3-film (6.1%) versus the n1-film (5.2%), and AF values comprised between 10 and 13% can be expected for the n2, n4, and n5 films.

3. Morphological properties of AZO films

High-resolution TEM and STEM images have been acquired on n1 and n3-films. As the results for both samples are similar, only n3-film images are shown here [Figs. 6(a)–6(c)]. Cross-sectional HRTEM images confirmed the polycrystalline structure of the film. The crystallite size distribution is wide with values comprised between a few nanometers to 25 nm, and their shape is irregular. Some layers of disordered atoms can be seen separating the neighboring crystallites of different orientations that correspond to grain boundaries, but no nanolaminates structure can be distinguished such as in Wu *et al.* (T:D ratio = 1:85)[7] or Viter *et al.* [T:D ratio = x:x with x = (3;5;13;25;50)] works.[37] As the crystallite size is small, many grain boundaries are observed. The Fourier transform patterns obtained from the high angle annular dark field (HAADF) image shows ZnO (100), ZnO (101), ZnO (110), and ZnO (114 and/or 211) in agreement with GIXRD results.

4. Electrical properties of AZO films

The electrical properties as determined by Hall measurements are presented in Fig. 7. The Al sequence influences the carrier concentration (from 1 to 2×10^{20} cm^{-3}), the carrier mobility (from 2.5 to 4.1 $cm^2/V\,s$), and the overall resistivity (from 8.3 to 24.1×10^{-3} Ω cm). Those results are congruent with the reported values of ALD films of similar thicknesses and T:D ratio.[34,38]

TABLE I. Zn, Al, and O contents for n1 and n3 films determined from TEM-EDS measurements with an absolute error of 1 at. % (for O and Al) or smaller (for Zn) but with a relative precision of 0.1 at. % when comparing the two samples.

Samples	%Zn	%O	%Al	%O/(%Zn + %Al)	AF_{TEM} (%)
n1	44.3	50.5	5.2	1.02	10.5
n3	39.9	53.9	6.1	1.17	13.3

5. Optical properties of AZO films

The transmittance spectra of the AZO films grown on borosilicate glass from the five Al sequences are presented in Fig. 8(a). The films are relatively transparent, with transmittance values comprised in the range [77; 87]% in the visible light region and as high as 89% in the NIR region, modulated by interference effects. The five curves are nearly superposed over a large wavelength range from 500 up to 1300 nm but differ in the NIR region with a relative order transmittance (% in NIR): n3 > n2, n4 > n5 > n1.

Absorption coefficients (α, in cm^{-1}) of the films were determined from the transmittance (T) and the reflectance (R) spectra using the formula $\alpha = -(1/th) \times \ln(T/(1 - R))$ with $T = T_F/T_G$ and $R = R_F - T \cdot R_G$, where th is the film thickness, T_F and R_F the transmittance and the reflectance of the film, and T_G and R_G the transmittance and the reflectance of the borosilicate glass substrate. Optical direct band gaps (E_g) were determined using the Tauc formalism[39] from the slope of $(\alpha \cdot E)^2$ as a function of E as depicted in Fig. 8(b). Band gap values between 3.54 and 3.64 eV are observed with the relative order n2 > n3,n5 > n1 > n4.

In summary, the main film characteristics from each Al sequences are reported in Table II.

IV. DISCUSSION

A. Impact of the Al sequence on the growth

Growth mechanisms occurring during the AZO deposition of the five Al sequences can be discussed based on GPMP and GPC values (Fig. 2), and *in situ* QCM monitoring [Fig. 3(c)]. Main reactions are ligand exchange between adsorbed metal-alkyl group and water or between adsorbed metal-hydroxyl group and metal alkyl precursor that both release alkane molecules. Two other phenomena, described in details elsewhere,[30,33,40,41] are in play: (1) the etching of

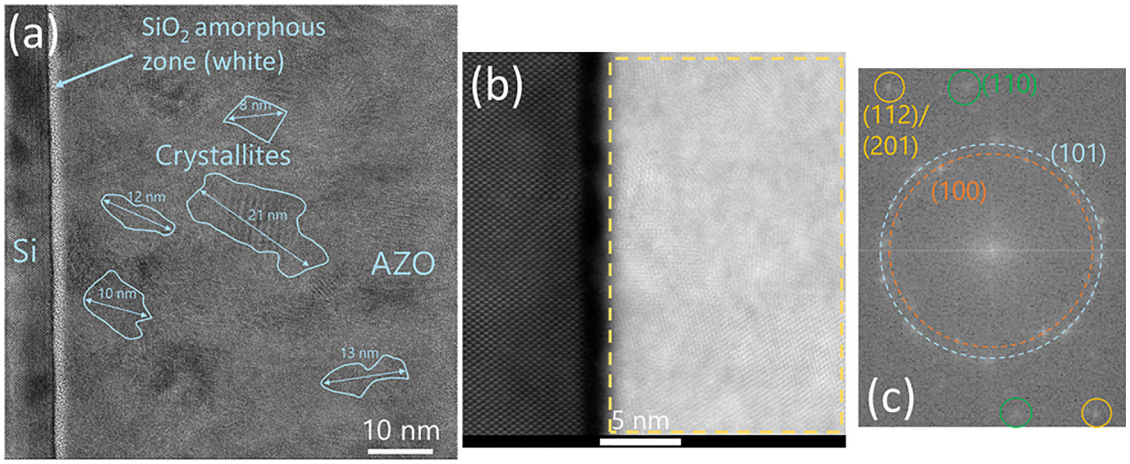

FIG. 6. (Color online) (a) Cross-sectional HRTEM image for n3-film. (b) Cross-section HAADF image for n3-film. (c) Corresponding lattice plane of the HAADF image determined by Fourier transform with their d-spacing value (Image J).

the Zn-alkyl surface species by the TMA (Refs. 30, 33, and 40) with the release of $Zn(CH_3)_2$ (Ref. 41) leading to a mass loss; (2) the relative stability of Al methyl group under DEZ exposure leading to a minor mass change.[30,40] Phenomenon 1 occurs when the TMA pulse follows a DEZ pulse (n1, n2, and n5 sequences), while phenomenon 2 is expected when the DEZ pulse follows a TMA pulse (n2 and n3 sequences). According to Fig. 3(c) and mass ratio calculations, the mass lost during the phenomenon 1 ($-90\,ng\,cm^{-2}$) is high enough to consider the desorption of C_2H_6 specie in addition to the $Zn(CH_3)_2$ released. The minor mass gain observed for phenomenon 2 [Fig. 3(c)] may be ascribed to the passivation of surface defect sites[31] or to the saturation of the last free hydroxyls terminated groups. These phenomena influence the film growth and thus explain the growth differences between the five Al sequences.

The n4 sequence, which alternates water pulses with metallic pulses, shows the highest GPMP, GPC, and mass uptake values. During the O-Zn cycles, the mass uptake of n4 sequence is similar to ZnO average mass uptake while during the Al doping cycle, the mass uptake is similar to Al_2O_3 average mass uptake. The Al doping cycle of n3 sequence contains an extra DEZ pulse that occurs after a TMA pulse. Mass uptake similar to n4 and slightly lower GPC are observed. This evidences that the impact of phenomenon 2 on the growth is indeed minor. N2 sequence displays the lowest GPMP, GPC, and mass uptake values. A large mass loss is observed during the TMA pulse ($-90\,ng/cm^2$), and only a small mass gain occurs during the following DEZ pulse ($+2.8\,ng/cm^2$). This value is similar to the ones observed in n3 sequence during the DEZ pulse of the Al doping cycle ($+2.5\,ng/cm^2$). That may indicate that the Al species adsorbed during the TMA pulse cover the same surface area whatever the preceding precursor pulse or that it generates a similar number of surface defect sites. In comparison with n1, n2 sequence has a DEZ pulse rather than a H_2O pulse after the TMA exposure that leads to lower GPC, GPMP, and mass uptake values. While the H_2O pulse for n1 is mostly adsorbed on Al species with a mass gain ($+7.5\,ng/cm^2$) similar to what is obtained for Al_2O_3 deposition ($+6.1\,ng/cm^2$), the DEZ pulse for n2 only adsorbed on remaining hydroxyl groups. Finally, n2 has less O-Zn cycles between each Al doping cycle. This explains the relative lower GPC (versus n1 and n5). Indeed, a lower mass uptake is observed during the five O-Zn cycles following an Al doping cycle compared to steady-state ZnO ALD.[30,33] This impacts more the overall GPC than the minor mass uptake that can be expected from phenomenon 2 (n2 versus n5). *In situ* QCM data of n1 and n5 sequences exhibit similar mass loss during the TMA pulse which was attributed to phenomenon 1. The additional H_2O pulse in n1 sequence allows an overall mass gain that is not high enough to lead to different GPC or GPMP values.

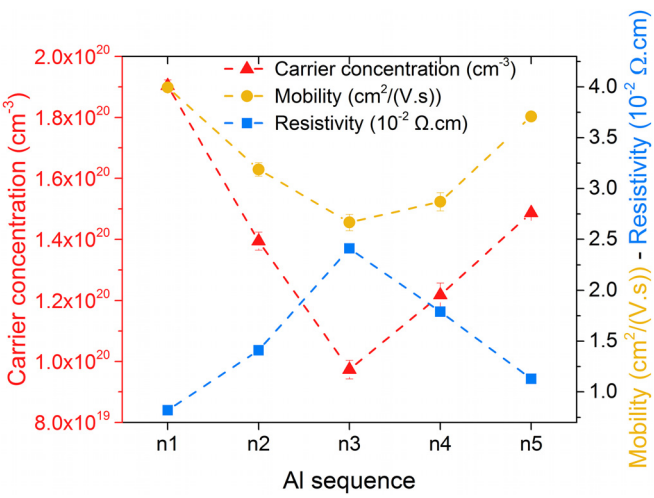

FIG. 7. (Color online) Carrier concentration, electrical mobility, and resistivity from Hall effect measurements as a function of the Al sequence. The dashed curves are a guide to the eye.

The influence of the deposition temperature on the mass variations was also investigated by conducting similar QCM studies for n1 and n3 sequences at $T_{dep} = 200\,°C$ [Figs. 9(a) and 9(b)]. The mass variations in the Al doping cycle, and especially for phenomena 1 and 2 were examined. At $T_{dep} = 200\,°C$, for n1 sequence, phenomenon 1 shows a higher etching rate while for n3 sequence, phenomenon 2 leads to a similar mass uptake than what is observed at 160 °C. Moreover for n3, during the

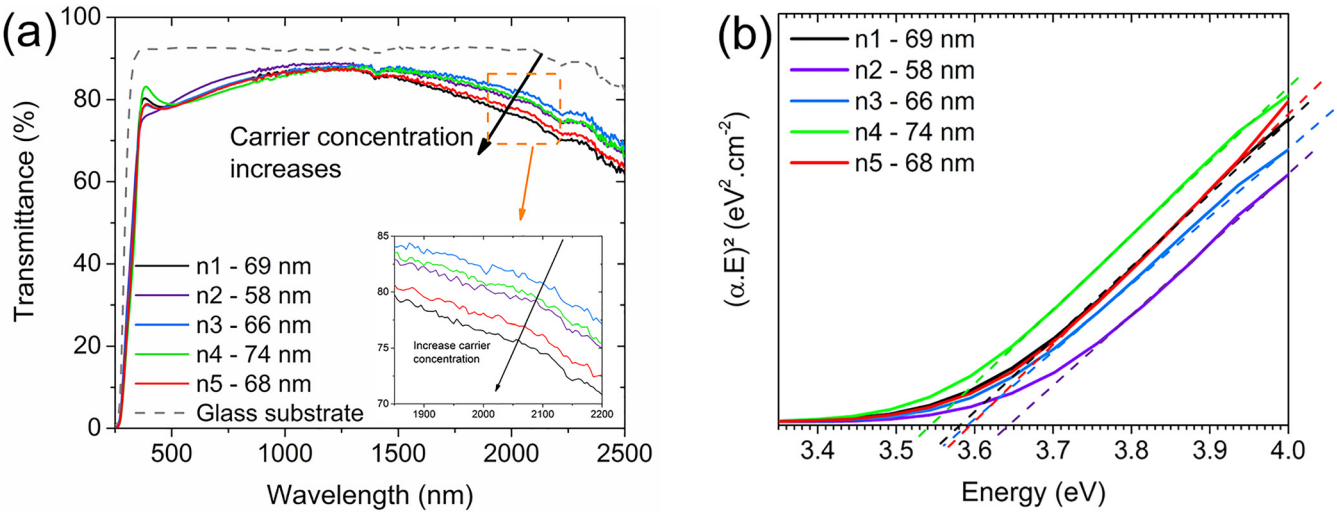

FIG. 8. (Color online) (a) Transmittance spectra of AZO films deposited on borosilicate glass for the five Al sequences with corresponding thicknesses. (b) Tauc plots. The dashed lines are a guide to the eye.

TMA pulse which follows a H_2O pulse, the mass uptake is slightly negative at 200 °C rather than positive. It was found that the mass variation differences during these phenomena observed from 160 to 200 °C are analogous to the tendency observed in other studies when the T:D ratio is increased.[30,33] Indeed, the 1:4 ratio compared to 1:10 and 1:19 T:D ratios shows a particularly higher mass loss during phenomenon 1 while it shows a mass loss rather than a mass gain when TMA pulse follows H_2O pulse[30] evidencing that when the T:D ratio increases, the etching phenomenon can also occur in this Al sequence case.[33] Na *et al*. have suggested that Al species are readily mixed in the ZnO layers by observing a switch of the dominant bonds from Zn-O to Zn-O-Al when the T:D ratio was increased.[30] The similarities of the results suggest that this intermixing improvement of Zn and Al species can also occur at a higher temperature. Indeed, the TMA precursor may be faster to react with the film when acquiring more energy from the substrate, leading to a substitution of a larger amount of Zn species.

This intermixing has been demonstrated to be beneficial for improving the electrical properties of AZO films[13,19] and in our case the n1-film shows a lower resistivity (3.5×10^{-3} Ω cm) when grown at 200 °C.

B. Influence of the Al sequence on the film properties

The Al sequence has only a small impact on the film crystalline properties as GIXRD patterns display only small differences (Fig. 4). It can be explained by the similar or only weakly distinct values of the parameters that have been reported to impact the ALD-AZO patterns: deposition temperature as it determines the amount of residual alkyl groups into the film[19] and Al doping content.[34] A shift of the disturbed (100) and (110) planes positions versus undoped ZnO was observed for all films, and depends on the Al sequence. This lattice plane distance modification is related to Al incorporation in the cell because of its smaller atomic radius compared to Zn atoms.[34] The highest angular peak positions are observed for n3 sequence while peaks for n1 sequence have the lowest angular positions. Thus, it can be assumed that n3 sequence leads to the highest Al incorporation rate per metal pulse while n1 has the lowest, which is corroborated by EDS measurements.

The electrical properties are mainly influenced by the deposition temperature and the Al content in the films.[10,42] For high T:D ratio 1:10, the solubility limit of Al in the ZnO matrix, i.e., Al_{Zn}^{+}, is probably exceeded,[10] as the Al sequence leading to the film with the highest Al content does not exhibit the highest carrier concentration, and the five Al sequences cannot be ranked in the same order for Al content and carrier concentration. Thus, the carrier concentration in the n1-film is higher than that in the n3-film while the Al content has been shown to be 1% smaller by TEM-EDS. The atoms that are not acting as dopants are assumed to act as traps for free carriers when segregating from the bulk in the grain boundaries,[7,43] which could partly explain the resistive behavior of n3. However, direct TEM observations could not

TABLE II. Main characteristics of AZO films grown using the five Al sequences.

	Al sequence	Thickness (nm) ± 1	GPMP (Å/metallic pulse)	Resistivity (10^{-3} Ω cm)	Carrier concentration (10^{19} cm^{-3})	Band gap (eV) ± 0.03	AF_{SEM}
n1	TMA/H_2O	69	1.57	8.3	19 ± 0.2	3.58	8.1
n2	TMA/DEZ	58	1.31	14.1	14 ± 0.3	3.64	9.8
n3	H_2O/TMA/DEZ	66	1.50	24.1	9.7 ± 0.3	3.59	9.8
n4	H_2O/TMA	74	1.69	17.9	12 ± 0.4	3.54	9
n5	TMA	68	1.54	11.3	15 ± 0.1	3.59	8.2

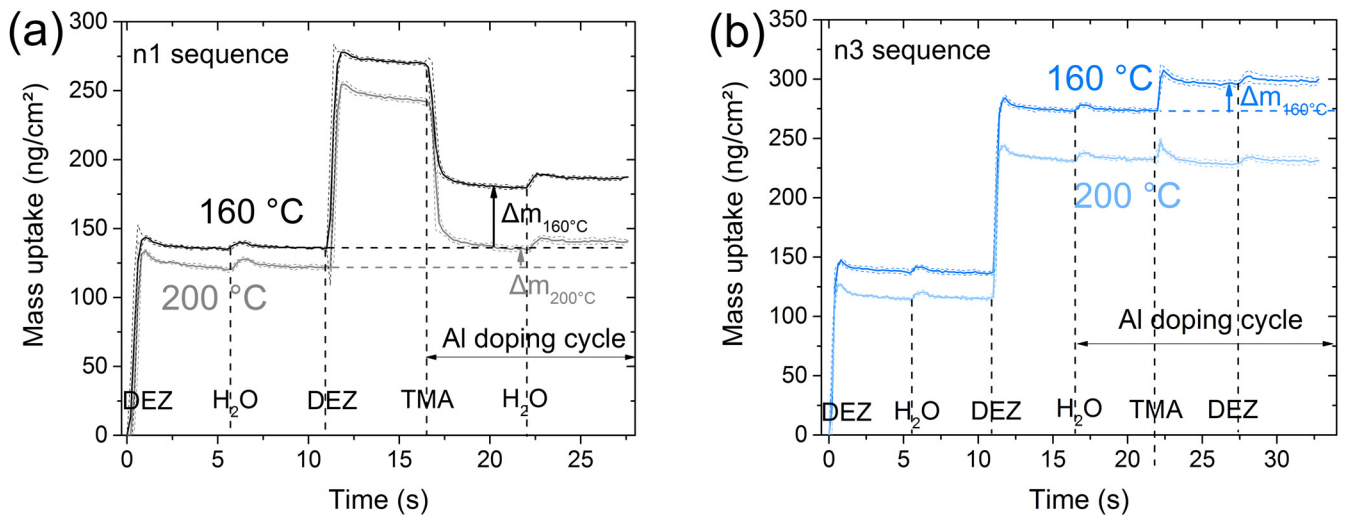

FIG. 9. (Color online) Mass uptake as a function of time during the Al doping cycle (a) for n1 sequence and (b) n3 sequence grown at 160 and 200 °C with a T:D ratio of 1:10 using *in situ* QCM measurements.

confirm that hypothesis. The temperature dependent Hall effect measurements would allow determining trapping state density and energy barrier height.[44] Films with atomic contents $O/(Al+Zn)>1$ can suggest the presence of other phases such as insulating AlO_x clusters, but as those were not observed by TEM, extra O atoms may be in interstitial sites O_i and act as traps (acceptor-type) for carriers. It would both explain the low carrier concentration and relative high electrical resistivity of the n3-film.

The resulting films of n3 and n4 sequences were already shown to have similar thicknesses and Al/Zn ratios (for T:D = 1:19 ratio).[30] Our growth study suggests indeed comparable Al incorporation as the mass uptake is similar during their respective Al doping cycle, yet an higher AF ratio was measured by SEM-EDS for the n3-film [Fig. 4(b)] and may be explained by a reduced amount of Zn concentration in the film. Indeed, the extra DEZ pulse in the Al doping cycle does not affect significantly the growth for the n3 sequence, and so only a low amount of Zn atoms may be incorporated during this step. In contrast, for the n4 sequence, metallic pulses are not affected by growth phenomena 1 and 2 and, according to EDS measurements, lead approximately to a film composed of one Al atom for 10 Zn atoms [Fig. 5(a)], which can be explained by an equal contribution of TMA and DEZ pulses to the amount of deposited atoms. n2-AF_{SEM} is as high as n3-AF_{SEM} [Fig. 5(a)] and can also be explained by a lower [Zn] than in films grown with other Al sequences (especially n4) due to phenomena 1 and 2 that either etch Zn species or prevent their adsorption. N5-film has been observed to have a lower Al concentration than n3 and n4-films when grown at 125 °C.[30] In our study, n1-AF_{SEM} is even lower than n5-AF_{SEM} [Fig. 5(a)] which means that the second H_2O pulse following the TMA pulse may either reduce the Al adsorption in the film or improve the adsorption of the next DEZ molecules. The second assumption is highlighted by the fact that n1-film contains more free carriers than n5-film. As already mentioned, for a high T:D ratio like in this study, a reduced [Al] improves the electrical properties. Thus, the film grown by the n1 sequence may have a higher [Zn], due to an improved DEZ adsorption during the first O-Zn cycles enhanced by the two successive H_2O pulses. According to QCM measurements, GPC of the n1 sequence is however not higher for the first O-Zn cycle but is for the second O-Zn cycle compared to n5 sequence with a mass gain of $101.7\,ng\times cm^{-2}$ vs $95.7\,ng\times cm^{-2}$. Two following identical precursor doses have already been used in ALD to improve GPC of the binary materials.[45,46] N1 sequence shows a similar GPC/GPMP, while having an improved conductivity, mobility and free carrier concentration compared to the n5 sequence. Thus, the n1 sequence may also be considered as an Al sequence of interest for depositing films similar to n5-films which are already used for some applications.[13,27,28] When grown at 160 °C, the n5-film has a lower resistivity than the n2-film. Pollock and Lad have shown the contrary for films grown at 200 °C, with a closed T:D ratio (1:12) and similar thicknesses.[31] They reported an increase in the (002) orientation with the n2 sequence compared to n4 and n5 sequences at 200 °C and presumed that DEZ molecules from the DEZ pulse following the TMA etching step fill surface defect sites. The Zn species adsorption might also prevent the AlO_x cluster formation by creating a Zn-Al-O intermixed and contribute to the larger (002) grain growth of the n2-film as observed by Pollock and Lad, which are beneficial for its electrical properties and so would explain why n2-film is less resistive than n5-film when grown at 200 °C.

At $T_{dep}=160$ °C, n1, n2, and n5 sequences have the best electrical properties compared to n3 and n4: lower resistivity and higher mobility. As mentioned by Na *et al.*, with a 1:10 T:D ratio at 125 °C, DEZ introduced previous to TMA pulse leads to a reduced number of adsorption sites for Al.[30] Thus, the relative better electrical properties for n1, n2, and n5 are likely due to a lower Al content, closer to the optimal one, i.e., preventing the formation of resistive Al_2O_3 phases. In other words, reducing the Al doping packing by inhibiting Al adsorption is a powerful method to improve conductivity.

Indeed, n5 sequence has been demonstrated to improve Al doping uniformity and to avoid metallic Al cluster formation in the nanolaminate structure compared to the n4 sequence.[29] This explains the recent improvement in terms of AZO film quality reported by authors choosing the n5 sequence.[13,27,28] Similar strategies have been reported by Yanguas-Gil *et al.* that employed alkyl alcohol previous to TMA pulse to partially inhibit Al adsorption[47] or Kim *et al.* that used the passivation effect of titanium tetra isopropoxide toward the chemisorption of TMA to reduce the Al/Ti average ratio for Al-doped TiO_2 thin films.[48]

From the optical properties of the films [Fig. 8(a)], using the Drude model[49] for free-carrier absorption, it can be confirmed that the transmittance values in the NIR range are consistent with the electrical properties of the films. While having the highest transmittance in the NIR, n3 and n4 sequences present the lowest carrier concentration in contrast with n1 and n5 sequences which present the lowest transmittance in the NIR but the highest carrier concentration.

According to the Burstein-Moss effect[50] in the UV range, the shift of the transmittance in the UV absorption edge is proportional to the optical band gap size as determined using the $(\alpha \cdot E)^2$ plot [Fig. 8(b)]. The n2 sequence led to the wider band gap, n4 to the lowest while n1, n3, and n5 band gaps are similar within the error. Comparisons with 1:20 and 1:40 T:D ratios (not depicted here) also clearly show that the n2-film has the largest band gap among the five films while they have similar thicknesses, and on the contrary, the n4-film has one of the lowest band gap for the three ratios. In summary, the band gap value depends on the Al sequence since it has an effect on the carrier concentration and on the film composition. However, a direct correlation between the band gap and carrier concentration is not observed here for the five films of the same 1:10 T:D ratio. Vegard's law gives values of the same order of what is obtained: 3.53 eV for n1 and 3.59 eV for n3, confirming the global correlation between Al content and band gap but it does not explain the small discrepancies between the Al sequences. A possible explanation is the local formation of a large band gap metastable phase, such as $(ZnO)_3(Al_2O_3)$ in the environment of the Al atoms in the supersaturated solid as reported by Yoshioka *et al.*[51] According to Wu *et al.*, for $AF_{EDS} > 7\%$, the optical band gap shift has a larger variation than the Fermi level shift suggesting the presence of AlO_x clusters inside the films that impact the optical bad gap[7]. Al_2O_3 phase having a large band gap ($E_g \approx 6$–7 eV) compared to ZnO so that it might cause the increase in the optical band gaps of AZO films. Thus, the n2 sequence (DEZ-TMA-DEZ pulse order) might enhance the local formation of one of this large band gap metastable phase which might have a strong effect on the band gap size and be absent from the n4-film.

V. SUMMARY AND CONCLUSIONS

ALD is a thin film deposition technique based on self limited surface reactions. This study has highlighted the impact of the pulse order during the Al doping cycle on the AZO film growth and overall final properties.

Five Al sequences were tested for a given [pulse number of TMA]:[pulse number of DEZ] ratio (T:D = 1:10) at a deposition temperature of 160 °C. Aside from ligand exchanges/loss mechanisms, two phenomena explaining the mass variations during the growth could be identified by *in situ* QCM measurements. When a TMA pulse follows a DEZ pulse, the observed mass loss was attributed to the etching of the Zn-alkyls surface species. When DEZ follows TMA, similar etching reactions are not thermodynamically favorable and the minor mass gain was attributed to the saturation of free hydroxyl groups or to the passivation of the surface defect sites. Surface reactions of the TMA precursor on the favorable –OH surface groups and on $–Zn-(C_2H_5)^*$ were shown to be temperature dependent when comparing growth mechanisms at 160 and 200 °C for two Al sequences. The increase in temperature was shown to have a similar impact than when the T:D ratio is increased, probably because of an improved intermixing between the Al species and ZnO layers. Better electrical properties were obtained when the DEZ pulse precedes the TMA pulse, by reducing the Al incorporation per cycle. The composition and optical properties also appeared to be highly dependent on the Al sequence while the structural properties are less impacted. A higher band gap size was obtained when the TMA pulse is between two DEZ pulses but no correlation with Al incorporation was revealed suggesting the presence of cluster dependency that would widen the optical band gap.

In summary, the sequence precursor introduction for the ALD deposited multinary films is a parameter that must be carefully chosen, as it dictates the chemical surface reactions and influences the final properties of the thin films.

ACKNOWLEDGMENTS

The authors would like to thank the French Environment and Energy Management Agency (ADEME) and EDF for their financial support, and David Troadec (IEMN Lille University) for preparing the TEM specimens by FIB. Purchase of the electronic microscope has been funded by the French National Research Agency (ANR), Project TEMPOS, Contract No. 10-EQPX-0050, in the frame of the Equipex "Investissements d'Avenir" programme.

[1]P. Barquinha, R. Martins, L. Pereira, and E. Fortunato, *Transparent Oxide Electronics: From Materials to Devices* (Wiley, West Sussex, 2012).
[2]K. Ellmer, Nat. Photonics **6**, 809 (2012).
[3]C. Jagadish and S. J. Pearton, *Zinc Oxide Bulk, Thin Films and Nanostructures: Processing, Properties, and Applications* (Elsevier, London, 2006).
[4]K. Ellmer, A. Klein, and B. Rech, *Transparent Conductive Zinc Oxide: Basics and Applications in Thin Film Solar Cells* (Springer Science & Business Media, New York, 2007).
[5]L. Ding, S. Nicolay, J. Steinhauser, U. Kroll, and C. Ballif, Adv. Funct. Mater. **23**, 5177 (2013).
[6]J. L. Vossen, J. Electrochem. Soc. **126**, 319 (1979).
[7]Y. Wu, P. M. Hermkens, B. W. H. van de Loo, H. C. M. Knoops, S. E. Potts, M. A. Verheijen, F. Roozeboom, and W. M. M. Kessels, J. Appl. Phys. **114**, 024308 (2013).
[8]M. Ohyama, H. Kozuka, and T. Yoko, J. Am. Ceram. Soc. **81**, 1622 (1998).
[9]K. Ravichandran, N. Jabena Begum, S. Snega, and B. Sakthivel, Mater. Manuf. Processes **31**, 1411 (2016).

[10]T. Tynell and M. Karppinen, Semicond. Sci. Technol. **29**, 043001 (2014).
[11]M. A. L. Johnson, S. Fujita, W. H. Rowland, W. C. Hughes, J. W. Cook, Jr., and J. F. Schetzina, J. Electron. Mater. **25**, 855 (1996).
[12]C. S. Hwang, *Atomic Layer Deposition for Semiconductors* (Springer US, Boston, MA, 2014).
[13]M.-L. Lin, J.-M. Huang, C.-S. Ku, C.-M. Lin, H.-Y. Lee, and J.-Y. Juang, J. Alloys Compd. **727**, 565 (2017).
[14]J. R. Bakke, K. L. Pickrahn, T. P. Brennan, and S. F. Bent, Nanoscale **3**, 3482 (2011).
[15]V. Miikkulainen, M. Leskelä, M. Ritala, and R. L. Puurunen, J. Appl. Phys. **113**, 021301 (2013).
[16]S. M. George, Chem. Rev. **110**, 111 (2010).
[17]W. Niu, X. Li, S. K. Karuturi, D. W. Fam, H. Fan, S. Shrestha, L. H. Wong, and A. I. Y. Tok, Nanotechnology **26**, 064001 (2015).
[18]G. Luka, M. Godlewski, E. Guziewicz, P. Stakhira, V. Cherpak, and D. Volynyuk, Semicond. Sci. Technol. **27**, 074006 (2012).
[19]C. H. Ahn, S. Y. Lee, and H. K. Cho, Thin Solid Films **545**, 106 (2013).
[20]D.-J. Lee, J.-Y. Kwon, S.-H. Kim, H.-M. Kim, and K.-B. Kim, J. Electrochem. Soc. **158**, 277 (2011).
[21]P. Genevée, F. Donsanti, G. Renou, and D. Lincot, Appl. Surf. Sci. **264**, 464 (2012).
[22]H. K. Park, B. S. Yang, S. Park, M. S. Kim, J. C. Shin, and J. Heo, J. Alloys Compd. **605**, 124 (2014).
[23]H. Yuan, B. Luo, D. Yu, A. Cheng, S. A. Campbell, and W. L. Gladfelter, J. Vac. Sci. Technol. **30**, 01A138 (2012).
[24]Y. Wu, S. E. Potts, P. M. Hermkens, H. C. M. Knoops, F. Roozeboom, and W. M. M. Kessels, Chem. Mater. **25**, 4619 (2013).
[25]X. Qian, Y. Cao, B. Guo, H. Zhai, and A. Li, Chem. Vap. Deposition **19**, 180 (2013).
[26]M. Li, X. Qian, A.-D. Li, Y.-Q. Cao, H.-F. Zhai, and D. Wu, Thin Solid Films **646**, 126 (2018).
[27]Y.-J. Choi, S. C. Gong, D. C. Johnson, S. Golledge, G. Y. Yeom, and H.-H. Park, Appl. Surf. Sci. **269**, 92 (2013).
[28]J.-M. Huang, C.-S. Ku, C.-M. Lin, S.-Y. Chen, and H.-Y. Lee, Mater. Chem. Phys. **165**, 245 (2015).
[29]J. Y. Kim, Y.-J. Choi, H.-H. Park, S. Golledge, and D. C. Johnson, J. Vac. Sci. Technol. **28**, 1111 (2010).
[30]J.-S. Na, Q. Peng, G. Scarel, and G. N. Parsons, Chem. Mater. **21**, 5585 (2009).
[31]E. B. Pollock and R. J. Lad, J. Vac. Sci. Technol. **32**, 041516 (2014).
[32]R. C. Weast, M. J. Astle, and W. H. Beyer, *CRC Handbook of Chemistry and Physics: A Ready-Reference Book of Chemical and Physical Data* (CRC, Boca Raton, 1983).
[33]J. W. Elam and S. M. George, Chem. Mater. **15**, 1020 (2003).
[34]P. Banerjee, W.-J. Lee, K.-R. Bae, S. B. Lee, and G. W. Rubloff, J. Appl. Phys. **108**, 043504 (2010).
[35]M. Birkholz, P. F. Fewster, and C. Genzel, *Thin Film Analysis by X-Ray Scattering* (Wiley-VCH, Weinheim, 2006).
[36]D. Abou-Ras, T. Kirchartz, and U. Rau, *Advanced Characterization Techniques for Thin Film Solar Cells* (Wiley VCH, Weinheim, 2011).
[37]R. Viter *et al.*, J. Phys. Chem. C **120**, 5124 (2016).
[38]C.-H. Zhai, R.-J. Zhang, X. Chen, Y.-X. Zheng, S.-Y. Wang, J. Liu, N. Dai, and L.-Y. Chen, Nanoscale Res. Lett. **11**, 407 (2016).
[39]J. Tauc, R. Grigorovici, and A. Vancu, Phys. Status Solidi B **15**, 627 (1966).
[40]E. B. Yousfi, *Etude de La Croissance de Couches Minces D'oxydes (ZnO, Al_2O_3) et de Sulfures (ZnS, In_2S_3) Par La Méthode de Dépôt Chimique En Phase Vapeur À Flux Alternés (ALE): Etude Par Microgravimétrie À Quartz et Application À La Réalisation Des Cellules Solaires À Base de Cu(In,Ga)Se_2* (Université Pierre et Marie Curie (UPMC), Paris, 2000).
[41]J. W. Elam, J. A. Libera, M. J. Pellin, and P. C. Stair, Appl. Phys. Lett. **91**, 243105 (2007).
[42]M. Moret, A. Abou Chaaya, M. Bechelany, P. Miele, Y. Robin, and O. Briot, Superlattices Microstruct. **75**, 477 (2014).
[43]K. Ellmer and R. Mientus, Thin Solid Films **516**, 4620 (2008).
[44]J. Y. W. Seto, J. Appl. Phys. **46**, 5247 (1975).
[45]S. K. Sarkar, J. Y. Kim, D. N. Goldstein, N. R. Neale, K. Zhu, C. M. Elliott, A. J. Frank, and S. M. George, J. Phys. Chem. C **114**, 8032 (2010).
[46]T. Muneshwar and K. Cadien, J. Appl. Phys. **119**, 085306 (2016).
[47]A. Yanguas-Gil, K. E. Peterson, and J. W. Elam, Chem. Mater. **23**, 4295 (2011).
[48]S. K. Kim, G.-J. Choi, and C. S. Hwang, Electrochem. Solid-State Lett. **11**, G27 (2008).
[49]J. I. Pankove, *Optical Processes in Semiconductors* (Dover Publications, Inc, New York, 1971).
[50]E. Burstein, Phys. Rev. **93**, 632 (1954).
[51]S. Yoshioka, F. Oba, R. Huang, I. Tanaka, T. Mizoguchi, and T. Yamamoto, J. Appl. Phys. **103**, 014309 (2008).